



S cone increments and decrements: Nearly-linear perceptual scales and variable noise

Yangyi Shi, Rhea T. Eskew Jr. *

Department of Psychology, Northeastern University, Boston, MA 02115, USA

ARTICLE INFO

Keywords:

S cone
MLDS
Perceptual scale
S ON
S OFF
Variable noise
Increment
Decrement

ABSTRACT

Two psychophysical experiments investigated perceptual differences between increases and decreases in stimulation of the short-wavelength (S) cone photoreceptors. In Experiment 1, observers' suprathreshold perceptual scale responses to S cone stimulation were estimated using the Maximum Likelihood Difference Scaling (MLDS) procedure. In Experiment 2, observers' pedestal discrimination thresholds were measured with a two alternative forced choice (2AFC) method. Both experiments were performed using incremental (S+) and decremental (S-) contrasts separately. Substantial asymmetry between S+ and S- was found in pedestal discrimination thresholds, but not in S+ and S- perceptual scales: perceived S cone contrast was nearly linear with S cone contrast for both polarities. To reconcile perceptual scales and thresholds, a model is proposed in which the noise in the S cone pathway is assumed to be proportional to the square root of stimulus contrast. The model works well for both the perceptual scales and forced-choice discrimination, indicating that S+ and S- signals are processed in an asymmetrical way, likely due to the physiological differences between S ON and S OFF pathways.

1. Introduction

Humans possess three types of cone photoreceptors, each maximally sensitive to different wavelengths: short-wavelength (S), middle-wavelength (M), and long-wavelength (L) cones. S cones differ from L and M cones due to their smaller numbers, their distinctive distribution across the retina, their slower response kinetics, and in other ways (Baudin, Angueyra, Sinha, & Rieke, 2019; Smithson, 2014; Stockman & Sharpe, 2000). S cones have unique, asymmetrical post-receptoral pathways for processing incremental (S+) and decremental signals (S-) (Dacey, Crook, & Packer, 2014; Kim, Packer, & Dacey, 2024): that is, for test stimuli that either momentarily increase (S+) or decrease (S-) the quantal catch of the S-cones relative to their adapted level. Potential processing asymmetries between these two test polarities have attracted much attention in both psychophysical and physiological investigations.

McLellan and Eskew (2000) used a transient tritanopia paradigm to measure the detection thresholds of S+ and S- signals immediately after removing an adapting field. They found that immediately after extinguishing a short-wavelength adapting field, the S+ threshold was higher than the S- threshold. More generally, the action spectra for the effect of extinguishing adapting fields of varying wavelengths differed for S+ and

S- tests. Wang, Richters, and Eskew (2014) used bipolar, dynamic noise masks to raise S+ and S- detection thresholds, finding that compared to S- thresholds, S+ thresholds were more elevated by S, L + M and other noise masks. Gabree, Shepard and Eskew (2018) used the same test stimuli as Wang et al. (2014) but employed a pedestal discrimination paradigm. Their findings showed that the masking effect of S+ pedestals was stronger than that of S- pedestals. Like McLellan and Eskew (2000), Ijekah, Vanston, and Crognale (2019) found differences between S+ and S- field sensitivities, although as they noted, the differences they observed might be due to rod, not S cone, detection; rod intrusion is a potential concern in many studies of S-cone sensitivity since rods also show increment/decrement differences (Patel & Jones, 1968). However, McLellan and Eskew (2000) and Wang et al. (2014) included rod control conditions to rule out rod detection. Putting all of this together, these psychophysical studies suggest that S+ and S- signals are processed through separate visual mechanisms.

Assuming that S+ detection is based upon signals processed by ON pathways, and correspondingly by OFF pathways for S- detection (Dacey et al., 2014; Hartline, 1938; Schiller, 1992, 2010), the distinct psychophysical results for S+ and S- tests should arise from the differences between S cone ON and OFF pathways, which have asymmetrical anatomy and physiological responses. In retina, the S ON pathway

* Corresponding author at: Department of Psychology, Northeastern University, 360 Huntington Ave., Boston, MA 02115 USA.

E-mail address: r.eskew@northeastern.edu (R.T. Eskew).

begins with the “blue cone” ON bipolar cells. The S OFF pathways may begin with mid-ganglion bipolar cells (Dacey et al., 2014; Klug, Herr, Ngo, Sterling, & Schein, 2003; Patterson et al., 2019; Wool, Packer, Zaidi, & Dacey, 2019). At this bipolar cell level, horizontal cells connect both pathways with neighboring L and M cones, providing opposing L and M signals. These L and M signal inputs are also processed by the S ON and OFF pathways differently (Kim et al., 2024; Packer, Verweij, Li, Schnapf, & Dacey, 2010). At the next stage, distinct ganglion cells are involved in each pathway: S ON pathways connect to small bistratified ganglion cells and large bistratified ganglion cells. Both types of ganglion cells show a selective excitatory response to S+ signals. S ON pathways also connect to ON-mid-ganglion cells (Kim et al., 2024); while S OFF pathways connect to OFF-mid-ganglion cells (Klug et al., 2003; Wool et al., 2019). Differences between the ON and OFF pathways continue to be observed at the level of lateral geniculate nucleus (LGN) (Szmajda, Buzás, FitzGibbon, & Martin, 2006; Tailby, Solomon, & Lennie, 2008). Some of the physiological results also show differences between S ON and S OFF. In macaque monkey, contrast response of cells in the S ON pathway show more saturation than do S OFF pathway cells (Tailby et al., 2008); however, a more recent study in marmoset does not find this saturation difference (Eiber, Pietersen, Zeater, Solomon, & Martin, 2018).

In the current study, two psychophysical experiments were conducted to further investigate the asymmetry between S ON and OFF pathway, following a prior study that used achromatic test patches (Shi & Eskew, 2024). With achromatic stimuli, it was found that the increment perceptual scale (measured by Maximum Likelihood Difference Scaling or MLDS), was saturating (as found by Shooner and Mullen (2022) with grating patterns), and the decrement scale was a cubic function (similar to Whittle’s (1992) finding); forced-choice pedestal discrimination could be predicted by these scales, assuming that the noise in the system was constant at all contrasts. The present first experiment also used Maximum Likelihood Difference Scaling (MLDS), but here for S+ and S− tests, to measure the perceived magnitude of the stimuli. The resulting S+ and S− scales showed similar saturating and cubic nonlinear forms as in achromatic increments and decrements, although on average the S cone scales were much closer to linear than achromatic ones. The second experiment measured pedestal discrimination, revealing an asymmetrical pedestal discrimination pattern consistent with Gabree et al. (2018): discrimination thresholds were higher on S+ pedestals than on S− pedestals. Like for achromatic stimuli, S cone discrimination thresholds could be predicted from the perceptual scales (Shi & Eskew, 2024; Shooner & Mullen, 2022). However, unlike for achromatic stimuli, the prediction model for S cones was required to have internal noise that increases with contrast in order to allow the MLDS scale to correctly predict discrimination for S+ and S− stimuli.

2. Method

2.1. Observers

Four observers participated in the experiment, including two of the four observers from Shi and Eskew (2024) (YS and NT). They all had normal scores on both the Farnsworth-Munsell 100-hue test (Farnsworth, 1943) and the Hardy Rand and Rittler (HRR) Pseudoisochromatic Plates test, and NT had normal Rayleigh matches. Observers all had normal or corrected-to-normal acuity. Their non-dominant eye was patched. Non-emmetropes viewed the screen through an ophthalmic trial lens, mounted 13 mm in front of the dominant eye.

The current study was approved by the Northeastern University Institutional Review Board, and all observers provided informed consent.

2.2. Apparatus

The computer used for stimulus control was an Apple Mac Pro (Cupertino, CA), running OS X EI Capitan (version 10.11.6). Two Sony GDM-F520 CRT monitors (Tokyo, Japan) were used to collect data. The monitors’ radiance spectra, and intensity-nonlinearity functions, were measured with a Photo Research PR-670 spectroradiometer (Photo Research, Chatsworth, CA).

The first display (mean luminance of 104 cd/m²) failed after collecting data from two observers (AS and PB), and was replaced with the second identical one (calibrated to have a mean luminance of 53 cd/m²), to finish data collection. Both displays were sufficiently bright to saturate the rods (approximately 3.4 or 3.6 sct Td; M. Aguilar & Stiles, 1954).

A Bits# Display Controller (Cambridge Research Systems, Rochester, UK), with 14-bit intensity resolution for each color channel, was used to control the output color of the monitor; the intensity nonlinearity was corrected by loading a table into the Bits#. Both monitors’ refresh rates were 85 Hz.

2.3. Stimulus and experiment procedure

The stimulus and experimental procedure used in the experiment are the same as those in a previous study (Shi & Eskew, 2024), except that the stimulus chromaticities were S cone increments and decrements instead of achromatic increments and decrements. The S cone isolating RGB modulation was estimated empirically for each observer (see Appendix A) to ensure that L and M cone quantal catches were unaffected by stimulus presentation. As in the previous study, experiments were done on increments and decrements separately. Contrast is specified as $\Delta S/S$, with increments being positive and decrements negative.

Two experiments were carried out. Example trials of both experiments are shown in Fig. 1.

The first experiment used a Maximum Likelihood Difference Scaling (MLDS) procedure (Knoblauch & Maloney, 2008; Maloney & Yang, 2003). On each trial, four squares of the same polarity with different contrasts were presented on the screen (the ‘method of quads’). Observers were instructed to choose whether the top or bottom pair of squares appeared more similar to each other (see Fig. 1a and b). Among the four different contrasts, the two lower contrast values formed one pair, and the two higher contrast values formed the other. The positions of the pairs on the screen (top or bottom) and the positions of the squares within each pair (left or right) were randomized in every trial. The 11 contrast values were linearly sampled from twice the observers’ detection thresholds (measured in a preliminary experiment using method of adjustment), to the maximum contrast that the monitor could produce (S cone contrast of ± 0.745 for the first monitor, ± 0.864 for the second monitor). The experimental procedure included all possible combinations of selecting four contrasts out of the 11, resulting in 330 trials in a session. Observers repeated each session twice, and the data were pooled for analysis.

In the second experiment, a two-alternative spatial forced-choice (2AFC) pedestal discrimination method was employed as in Shi & Eskew (2024). During each run of 100 trials, all four squares presented had the same polarity (see Fig. 1c and d). Three of these squares served as pedestal stimuli, while the fourth was the test stimulus. The three pedestal-only squares had identical contrast, whereas the fourth square had an additional contrast (the test contrast); the test contrast could add to, or subtract from, the pedestal contrast (see Shi and Eskew (2024), their Fig. 3). At the beginning of each pedestal discrimination run, observers were instructed to attend to either the top or bottom pair of squares only and to select the target square that appeared more (or less) saturated in purple (or yellow) (Fig. 1c and d). In each trial, the target square was randomly positioned on the left or right side. The experiment employed a three-down-one-up staircase procedure (Wetherill & Levitt, 1965) to adjust the test contrast component over trials, with the pedestal

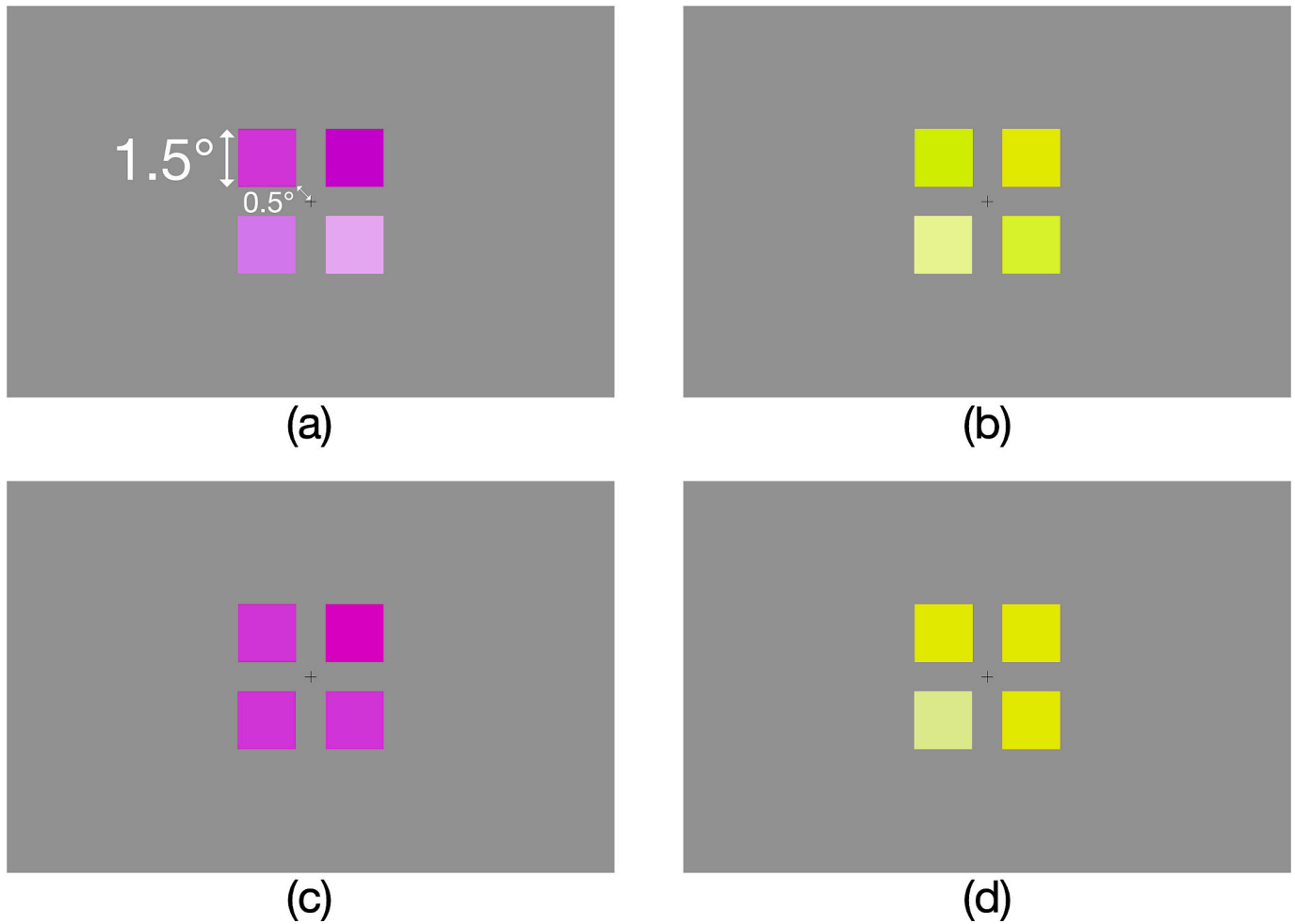


Fig. 1. Example trials of the two experiments. The spatial layout of the four-square patch was the same in both experiments. Each square has an edge length of 1.5° . The squares were 0.5° away from the fixation cross in the diagonal direction (see Shi & Eskew, 2024). (a-b) MLDS (Experiment 1, (a) S+; (b) S-). The four squares had the same polarity but different contrast magnitudes. The observers' task was to select either the top or bottom pair of squares as being more similar to one another. (c-d) pedestal discrimination (Experiment 2, (c) S+; (d) S-). The observer's task was to choose whether the test square was on the left side or the right side in the attended row (see text). (c) S+ pedestal and S+ test trial. The target square is on the right side, top row. (d) S- pedestal, S+ test trial. The target square is on the left side, bottom row.

contrasts kept constant for a run. The accumulated frequency of seeing data from the run were fit with a Weibull function and the threshold parameter (contrast at 82 % correct) obtained. All runs were repeated at least three times on at least two different days, and the mean threshold was calculated.

2.4. Analysis and model

The data collected in the two experiments were analyzed twice, under two assumptions: whether the internal noise is constant or variable.

Under the first assumption, where the noise standard deviation is constant, the original MLDS model (Knoblauch & Maloney, 2008; Maloney & Yang, 2003) was used to estimate the perceptual scale. The MLDS model is a difference scaling model developed based on the assumptions of signal detection theory (Wickens, 2002). In this framework, perceived contrast response is modeled as a normal distribution with a mean that is a monotonic function of contrast magnitude, and constant standard deviation. The perceptual scales estimated were then applied to a constant-noise prediction model (Shi & Eskew, 2024) to fit the pedestal discrimination data. Because this analysis with constant noise was incapable of predicting discrimination from the perceptual scale, only its main conclusions are described in the body of this paper;

the details are presented in Appendix B.

Under the second assumption, the noise is variable. Both the MLDS model and the prediction model were modified to include noise that increased monotonically with S cone contrast. Based upon trial calculations, the noise was assumed to have a standard deviation that is linearly related to the square root of the stimulus contrast, similar to the noise pattern of a Poisson distribution (Eq. (1), below).

3. Results

3.1. MLDS model with increasing noise

In this variable noise MLDS model, the perception of a contrast is a normal distribution with a mean corresponding to the perceptual scale value; the standard deviations of these normal distributions (the internal noise) increase with the square root of the contrast, as in Equation (1). C is the S cone contrast; $a_{S_{\pm}}$, $b_{S_{\pm}}$ are free parameters to be fit for increments and decrements separately (indicated by the + and - sign).

$$\sigma_{C,S_{\pm}} = a_{S_{\pm}} \times \sqrt{|C|} + b_{S_{\pm}} \quad (1)$$

The variable noise MLDS model, like the original constant-noise MLDS model, produces 11 mean perceptual scale values corresponding to the 11 contrast values, using the maximum likelihood method

(Knoblauch & Maloney, 2008; Maloney & Yang, 2003). It additionally fits the noise parameters $a_{S_{\pm}}$ and $b_{S_{\pm}}$. The perceptual scale values of lowest and highest contrasts were normalized to 0 and ± 1 . As in the original MLDS model, the decision variable in the variable noise MLDS model reflects the difference in perceptual differences between stimulus pairs, with variance determined by the summed variances of all four stimuli; unlike in the original MLDS model, these four variances are not identical, but depend upon the four contrasts.

The red points in Fig. 2 are the fitted results of the variable-noise MLDS model. Three observers (AS, PB, and YS) show a hint of saturation for the S+ scale at high contrasts, while NT's scale accelerates slightly at low contrast. All observers except AS show a clear suggestion of the cubic shape we observed for achromatic decrements, in which the scale values drop steeply for weak decrements, flatten slightly, then change steeply again (Shi & Eskew, 2024; Whittle, 1992). However, for all observers, both increment and decrement curves are closer to linear than the achromatic functions are – neither the saturating function for increments, nor the cubic function for decrements, show the degree of curvature that the analogous achromatic curves do (Shi & Eskew, 2024).

After the perceptual scale values were estimated by the variable noise MLDS model, increment scale values were fit with a modified Naka-Rushton equation (Eq. (2)), and the decrement scale values were fit with a cubic function (Eq. (3), as in Shi and Eskew (2024); the goal is to have a continuous, differentiable perceptual scale function. Both the modified Naka-Rushton equation and cubic function were constrained to pass through the first and last data points; see Appendix A of Shi and Eskew (2024) for a description of the constraints. In both equations, P

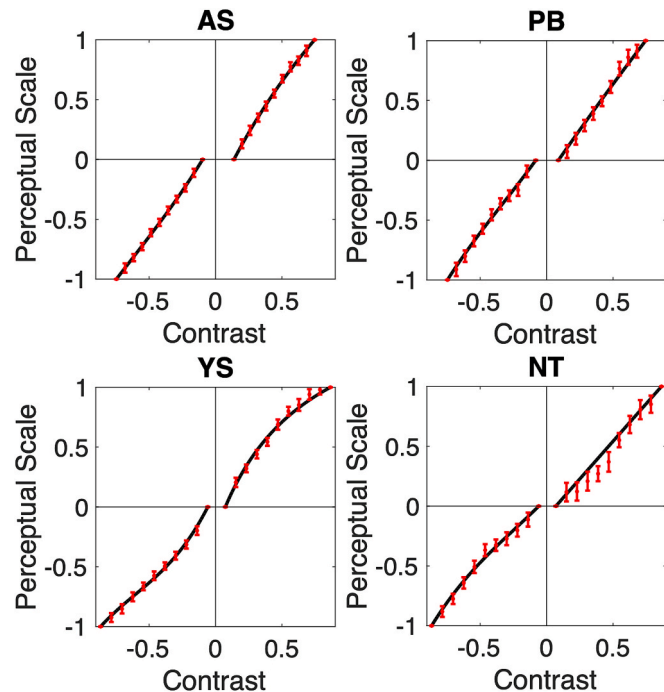


Fig. 2. The variable-noise MLDS model fitting results. S+ data are plotted in the first quadrant, and S- data are plotted in the third quadrant. The horizontal axis represents contrast, and the vertical axis represents estimated perceptual scale values. Positive and negative signs indicate contrast polarity (S+ or S-). Red data points show estimated perceptual scale values, and black curves represent the model fits: the modified Naka-Rushton equation (Eq. (2)) for increments and the cubic function for decrements (Eq. (3)). The data points closest to the origin correspond to contrast values set at twice the individual observer's detection threshold for that test polarity. Error bars indicate standard errors derived via bootstrapping. (For interpretation of the references to color in this figure legend, the reader is referred to the web version of this article.)

represents perceptual scale; C is the independent variable contrast; \pm represents stimulus polarity. In Equation (2), C_0 represents detection threshold contrast; C_{max} represents the maximum contrast (0.745 for the first monitor, 0.864 for the second monitor); m_+ a half-saturation constant, is the free parameter to be estimated. In Equation (3), n_1, n_2, n_3, n_4 are free parameters to be fit.

$$P_+ = \left[1 + \frac{m_+}{(C_{max} - 2C_{0+})} \right] \times \frac{(C_+ - 2C_{0+})}{(C_+ - 2C_{0+}) + m_+} \quad (2)$$

$$P_- = n_1 \times C_-^3 + n_2 \times C_-^2 + n_3 \times C_- + n_4 \quad (3)$$

3.2. Pedestal discrimination prediction model with increasing noise

The pedestal discrimination thresholds are presented as data points in Fig. 3. In both S+ and S- pedestal conditions, as the contrast magnitude increases, the discrimination threshold increases. However, discrimination thresholds increase faster on S+ pedestals than on S- pedestals. In particular, at the highest pedestal contrasts, the discrimination thresholds are higher on S+ than S- pedestals. This asymmetry between S+ and S- pedestal discrimination mirrors the findings of Gabree et al. (2018), who also observed higher discrimination thresholds for S+ pedestals at high contrast levels.

In the previous study (Shi & Eskew, 2024), a model was proposed that predicts achromatic discrimination thresholds based on the achromatic perceptual scale curve. However, that model assumed that the noise in the visual pathway is constant. The current study introduces a modified version of the model in which the noise is variable, rather than constant. Despite this change, the core principle remains the same: the discrimination threshold is inversely proportional to the local slope of the perceptual scale curve. In other words, if the perceptual scale changes slowly at a given pedestal contrast, the amount of test contrast required to make a discrimination should be large. Equation (4) summarizes this model, where C_t represents discrimination threshold contrast; $a_{S_{\pm}}$ and $b_{S_{\pm}}$ are the slope and intercept of the variable noise that were estimated by the MLDS model (Eq. (1)); the derivative $\frac{d}{dC} p(C_{ped})$ represents the slope of the perceptual scale curve at pedestal contrast C_{ped} . The only free parameter in the threshold prediction model is $k_{S_{\pm}}$, fit separately for S+ and S- pedestals.

$$C_t = k_{S_{\pm}} \times \left(a_{S_{\pm}} \times \sqrt{|C_{ped}|} + b_{S_{\pm}} \right) \times \frac{1}{\frac{d}{dC} p(C_{ped})} \quad (4)$$

The curves in Fig. 3 show the predictions from the variable noise model. Table 2 reports two measures of model fit: the squared correlation coefficient (R^2) and root-mean-square error (RMSE). The model fit is generally good for both increments and decrements for three observers; the fit is not as good for observer NT.

The fitted parameters of both variable noise MLDS model and prediction model are summarized in Table 1. The very large fitted value of the half-saturation constant m_+ for observer NT indicates that the Naka Rushton function fails to describe his S+ perceptual scale well.

Notice that although the intercepts of the noise equation (the b values in Eq. (1)) were freely fit, all the fitted results showed intercepts to be 0 or close to 0 (Table 1). This does not indicate the internal noise is zero when S cone contrast is actually zero, since the lower end of the contrast range used for MLDS was double the observer's detection threshold, not zero. Instead, the fact that b is at or near zero indicates that the dominant noise in these tasks is associated with suprathreshold contrasts (all the MLDS stimuli and the pedestals used for discrimination were suprathreshold).

The alternative, constant noise MLDS model described in Appendix B produced almost exactly the same perceptual scales, as shown in Fig. B2. However, this constant-noise model fails to account for discrimination (Fig. B3), for the following reason. Due to the almost linear perceptual scale in both polarities, the derivative is nearly constant, and using a constant noise standard deviation causes the predicted discrimination

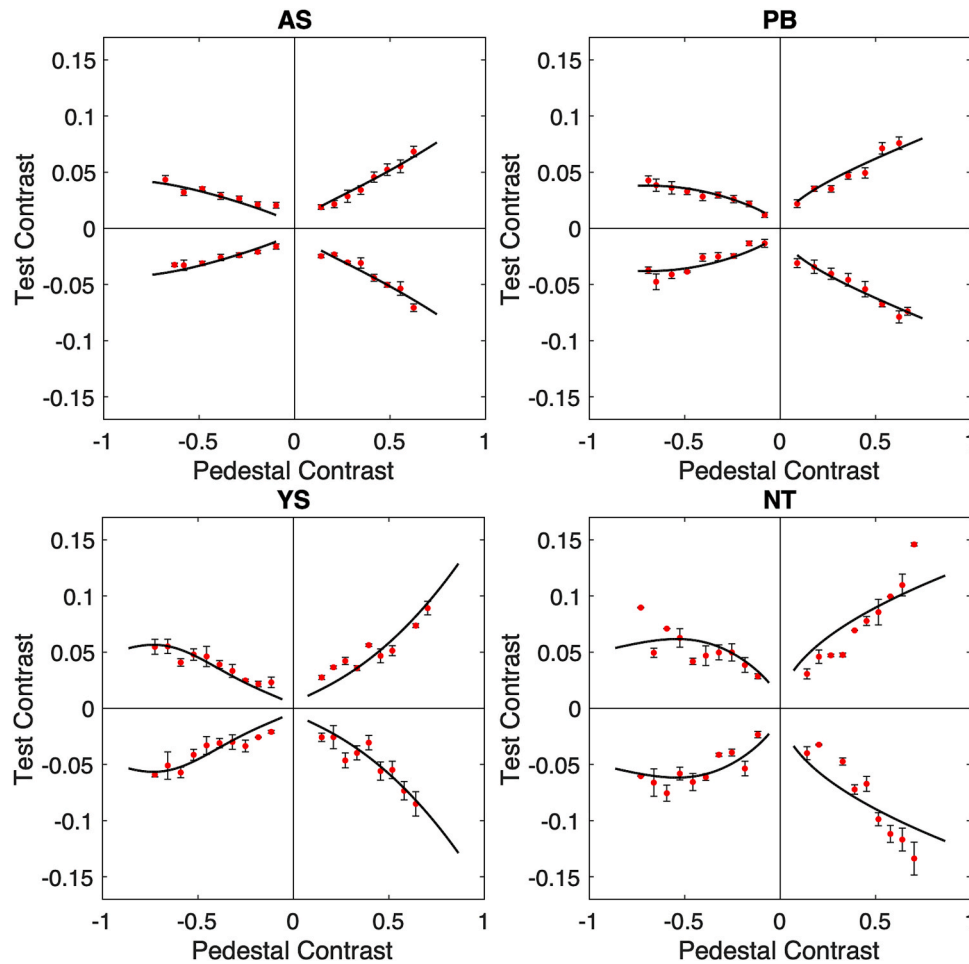


Fig. 3. Pedestal discrimination thresholds and model predictions from the variable noise model. In each panel, the horizontal axis represents pedestal contrast, and the vertical axis represents test contrast. The origin corresponds to zero contrast, representing the mid-grey background. Positive directions on both axes represent S+, and negative directions represent S-. For example, in the first quadrant, the pedestal condition is S+, and the test condition is S+. In the fourth quadrant, the pedestal condition is S+, and the test condition is S-.

Table 1
Parameters of variable noise models.

		AS	PB	YS	NT
S+	$\sigma_{C,S+}$				
	a_{S+}	0.114	0.183	0.093	0.244
	b_{S+}	0	0	0.013	0
S-	m_{S+}	2.064	8.329	0.701	319.745
	k_{S+}	0.989	0.718	0.766	0.654
	a_{S-}	0.102	0.174	0.108	0.155
S-	b_{S-}	0	0	0.002	0
	$n_{1,S-}$	0.418	0.523	1.134	0.597
	$n_{2,S-}$	-0.824	-0.531	-2.171	-0.406
	$n_{3,S-}$	1.970	1.620	2.335	1.137
	$n_{4,S-}$	-0.183	-0.128	-0.128	-0.065
	k_{S-}	0.673	0.430	0.587	0.661

Table 2
Measures of Goodness of fit to variable noise prediction model.

Condition/Observer	AS	PB	YS	NT
S+, R ²	0.95	0.92	0.77	0.72
S+, RMSE	0.004	0.005	0.009	0.018
S-, R ²	0.68	0.84	0.74	0.49
S-, RMSE	0.004	0.004	0.006	0.011

curves to be nearly flat – almost no masking – for observers AS, PB, NT, and thus fails to account for the observed thresholds. See Section 4.1 and 4.4 for related discussion.

4. Discussion

The current study measured observers’ scales for the perceived strength of S cone increments and decrements separately, using MLDS and pedestal discrimination. In the MLDS task, most observers produced perceptual scales that were close to linear in both S+ and S-, but in detail, most observers showed the same general form as previously found for achromatic increments and decrements: saturation for increments, a cubic function for decrements. The primary difference from the achromatic scales is that the derivatives of both S cone perceptual scale functions are of smaller magnitude.

In discrimination, all observers showed a strong asymmetry, with higher discrimination thresholds for S+ pedestals than for S- pedestals as pedestal contrast increased. This polarity difference is consistent with results from previous psychophysical studies (Gabree et al., 2018; McLellan & Eskew, 2000; Wang et al., 2014). Using the MLDS curves with the assumption of constant internal noise failed to predict the discrimination thresholds, unlike in the achromatic case (see Section 4.2). An alternative MLDS model was used, which assumed that internal noise increases with the square root of contrast; this model provided a good prediction of discrimination thresholds.

4.1. Constant and variable noise

MLDS is a difference scaling method that measures the differences in observers’ perception of stimulus pairs. Given the assumption that

internal representations of stimuli follow normal distributions, the perceptual scale values only correspond to the means of those distributions. Therefore, the estimated scale values (the means) are independent of whether the perceptual noise is constant or variable (Kingdom, 2016; Maloney & Yang, 2003). Thus changing perceptual noise from constant to variable (increasing with the square root of contrast) does not affect the estimated perceptual scale values: MLDS cannot determine the noise function (Kingdom, 2016).

Results from pedestal discrimination experiments alone also cannot unambiguously determine the magnitudes of internal noises. For example, Kontsevich, Chen, and Tyler's (2002) modeling of their psychophysical experiments suggested that internal noise should be variable; however, Georgeson and Meese (2006) later argued that a constant noise model could also explain Kontsevich et al.'s data well, since observers' performance depends, not on noise or signal, but on the signal-to-noise ratio. Other studies also addressed the flexibility of fitting both types of noise models to discrimination data sets (García-Pérez & Alcalá-Quintana, 2007, 2009).

However, as Kingdom (2016) argued, since MLDS is an "internal-noise-free" method for estimating perceptual scales, comparing these scales with those generated from discrimination tasks can help identify whether the noise is constant or variable, as shown in several other studies (G. Aguilar, Wichmann, & Maertens, 2017; Devinck & Knoblauch, 2012; Shooner & Mullen, 2022). In the current study, the constant noise prediction model (Fig. B2) shows much poorer agreement with the discrimination data, compared to the variable noise prediction model (Fig. 3). This suggests that for most observers (except perhaps observer YS for S+), the internal noise in the S cone channel is variable, increasing with contrast, while their perceptual scales in both increment and decrement pathways are close to linear.

In Shi and Eskew (2024), we used the constant-noise MLDS model to successfully predict pedestal discrimination functions for achromatic stimuli. Given that MLDS is transparent to the noise function, the question arises whether a variable-noise model could also be used for achromatic stimuli. On re-analysis of our achromatic data with noise varying as in Equation (1), the MLDS perceptual scales were completely unchanged, and the pedestal discrimination functions still fit the discrimination thresholds. The discrimination functions with increasing noise are shown in Fig. C2 in Appendix C, and Table C2 gives the new parameter values. However, most of the fitted slopes in the variable noise function (parameter a , Eq. (1)) are 0 or close to zero, meaning that despite allowing noise to grow with contrast, these estimated noises are in fact nearly constant, with a value given by the intercept (b , Eq. (1)). Therefore, this reanalysis suggests that for achromatic stimuli, the noise is in fact constant.

4.2. The crispening effect

Increasing perceptual differential sensitivity as absolute contrast approaches zero (i.e., near the adapting background) has been called the crispening effect (Takasaki, 1966; Whittle, 1992). It appears in the perceptual scale as a steepening near the origin. Previous studies that used achromatic contrast (Shi & Eskew, 2024; Shooner & Mullen, 2022; Whittle, 1992) found strong crispening effects in perceptual scales. This effect is barely visible in the present MLDS scales (Fig. 2).

On the other hand, the current discrimination results show the crispening effect—high sensitivity for weak pedestals (when pedestal contrasts are near the background). In the fitted variable noise model, high discrimination sensitivity near the origin is due to the smaller noise standard deviations at low contrasts, not to larger derivatives of perceptual scales or transducer functions at lower contrasts, because the derivatives remain largely unchanged (since the scales are close to linear). Because the perceptual scales are unaffected by the noise (Section 4.1), the perceptual scales themselves do not provide direct evidence for crispening in S cones.

4.3. Origins of the variable noise

Several studies have investigated the origins of noise in the visual pathway, providing compelling evidence for the presence of variable noise in sensory processing. Angueyra & Rieke (2013) identified the phototransduction process as a primary source of cone noise, driven by fluctuations in cGMP concentrations and gating transitions in ion channels, which are influenced by physiological conditions. Notably, they observed that this noise persists across different light levels, suggesting that while cone signals adapt to the ambient light, the noise itself remains, limiting sensitivity and introducing variability into the retinal output. Ala-Laurila et al. (2011) demonstrated that noise in retinal ganglion cells predominantly originates from cone photoreceptors, with correlated noise arising from shared cone inputs to neighboring ganglion cells. Crucially, this noise is not constant; its variability depends on the extent of shared input, indicating early fluctuations in the neural signal.

Consistent with these two results, Weber et al. (2021) provided direct evidence that noise in the visual pathway comprises both constant and variable components. They found that constant noise results from random fluctuations within the neural circuitry, whereas variable noise scales with stimulus intensity, increasing as the stimulus strengthens. This finding aligns with the predictions of current models, highlighting the role of variable noise in shaping neural responses and its significance in understanding perceptual decision-making.

Collectively, these studies suggest that variable noise generated at the retinal level constitutes a primary source of noise in the visual pathway and is closely tied to stimulus intensity. In the current model, variable noise is defined as the square root of stimulus contrast, effectively simulating a Poisson-like distribution and establishing a possible link to photon-related processes. Photoreceptor noise should be the same for our S+ and S− stimuli. The larger noise we found with S+ (MLDS and discrimination) could be taken to imply that more variability is added in ON than OFF post-receptoral pathways.

The question of why the relevant noise is constant in pathways serving achromatic vision but variable in pathways for S cone stimuli begs for future physiological study. It may be worth noting that magnocellular pathways may receive only limited S-cone input (Calkins, 2001; Chatterjee & Callaway, 2002; Sun, Smithson, Zaidi, & Lee, 2006), and if the achromatic performance measured in Shi and Eskew (2024) depended on magnocellular activity it might not be surprising that the noise model would differ between achromatic and S-cone tasks.

4.4. Model consequences of near-linear perceptual scales

Our discrimination model (Eq. (3)) has three terms that are multiplied together: a fitted constant k_{\pm} , the noise (proportional to the square root of contrast), and the derivative of the perceptual scale. The product of these last two terms represents the noise-to-signal ratio. When the perceptual scale is curved, the third term—the derivative—is not constant; that derivative thus contributes to the shape of the pedestal discrimination functions, whether the noise is constant or variable. When the second term—the noise—is constant, the derivative alone determines the pedestal discrimination function shape (as in Shi & Eskew, 2024). But to the extent that the perceptual scale is linear, as it nearly is here for three of the four observers, that third term is nearly constant; in this case the shape of the discrimination functions (Fig. 3) is (mostly) due to the noise function, which is the second term in the discrimination prediction model (Eq. (4)). The interplay of these two factors is a reflection of the fact that discrimination thresholds reflect the noise-to-signal ratio, rather than either alone.

The best fitting noise model parameters (a_{\pm} and b_{\pm} , Eq. (1)) differed for S+ and S− in our study. Forcing them to be the same for the two polarities produced almost identical predictions for the thresholds as those in Fig. 3, but caused the two k_{\pm} values to differ to a greater degree than in Table 1. This is again a reflection of the fact that when the perceptual scale derivative is nearly constant (Eq. (1)), the three

multiplicative terms can have offsetting effects. Linearity, or even near-linearity, in the estimated perceptual scale makes it difficult for the model to distinguish the origin of the changes in differential sensitivity with contrast.

4.5. Asymmetry between S cone ON and OFF pathways

An unexpected finding is that for most observers, large asymmetries between S+ and S- was observed most notably in pedestal discrimination, not in MLDS, where the polarity differences were relatively small. Gabree et al. (2018) found similar S cone pedestal discrimination asymmetry, in which as pedestal contrast increased, discrimination thresholds on S+ pedestals grew faster than on S- pedestals. They suggested that this asymmetry was due to differences in saturation and contrast gain control in the S cone ON and OFF pathways, consistent with results of Tailby et al. (2008) in macaque monkey.

However, Eiber et al. (2018) found that the differences between contrast response functions of S-ON and S-OFF cells in LGN to S cone isolating stimuli in the marmoset are small: both show linearity in the low to moderate contrast range, with only mild saturation in higher

contrast. One way to reconcile these different results is to suggest that the mean cell responses to different contrasts in the S-ON and S-OFF pathways may be similar, but the variability in response increases with contrast to a greater degree in the S-ON pathways than the S-OFF pathways.

CRediT authorship contribution statement

Yangyi Shi: Writing – review & editing, Writing – original draft, Visualization, Validation, Software, Resources, Project administration, Methodology, Investigation, Formal analysis, Data curation, Conceptualization. **Rhea T. Eskew:** Writing – review & editing, Validation, Supervision, Funding acquisition, Formal analysis, Conceptualization.

Acknowledgments

The authors thank Peyton Benz, Audrija Sarkar, and Nicholas Trent for serving as observers. Supported by a grant from the National Science Foundation (BCS-2239356).

Commercial relationships: none.

Appendix A. S cone isolating direction

We determined the relative amounts of red, green, and blue modulations on the monitor that isolated each observer's own S cones, using the method of silent substitution (Estévez & Spekreijse, 1982). The method used to determine S cone isolation was similar to that used in previous studies (Gabree et al., 2018; McLellan & Eskew, 2000; Wang et al., 2014; Webster & Mollon, 1994).

A "standard" S cone isolating direction, based upon the Stockman and Sharpe (2000) cone fundamentals, and a set of eight other potential directions, were tested with each of our observers. The additional RGB color directions were defined by varying macular pigment optical density (MPOD) and photopigment optical density (PPOD); for the young observers in this study, these two are likely to be the most important individual difference factors (He, Taveras-Cruz, & Eskew, 2021).

The observers used the method of adjustment to vary the contrast to threshold of an 1°-diameter disc filled with each candidate RGB, against the same uniform gray background field used in the main experiment. For observers AS and PB this was done with the first, brighter monitor; for observers NT and YS, it was done with the second, dimmer monitor. Thresholds were measured both with a 420 nm violet field covering the stimulus, and without the field (in both cases through a beamsplitter; see Fig. A1). The 420 nm field dilutes the contrast produced in the S cones by about 4x more than the L or M cone contrasts. The color direction that had the largest ratio between thresholds taken with and thresholds taken without the violet field was used as a first approximation to the S cone isolating direction; the whole procedure was then repeated with new MPOD and LPOD values, now varying around the first approximation values rather than the standard ones. The RGB with the highest threshold elevation produced by the violet field in this second stage was taken as the isolating direction. The color directions (RGB modulations) estimated to isolate S cones for each observer are given in the panels of Fig. A2.

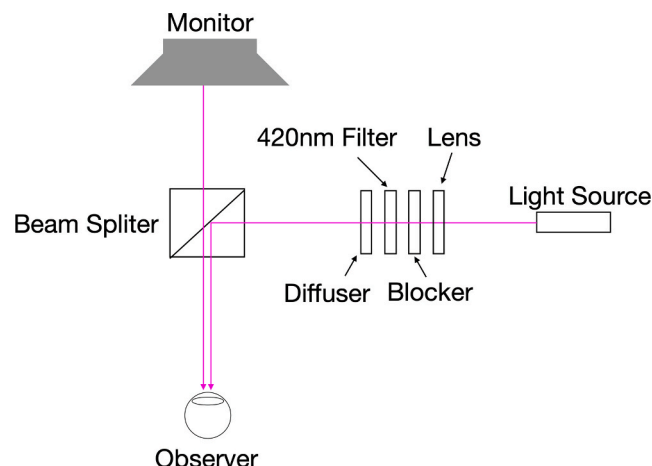


Fig. A1. Apparatus for finding the S cone isolating direction (not to scale). Light generated from a tungsten filament bulb was first collimated by a lens. It was then filtered by a 420 nm narrow-band interference filter. The beam was passed through a diffuser to create a uniform circular violet patch that appeared to cover the stimulus on the monitor. On trials without violet field, the light from the tungsten filament was blocked.

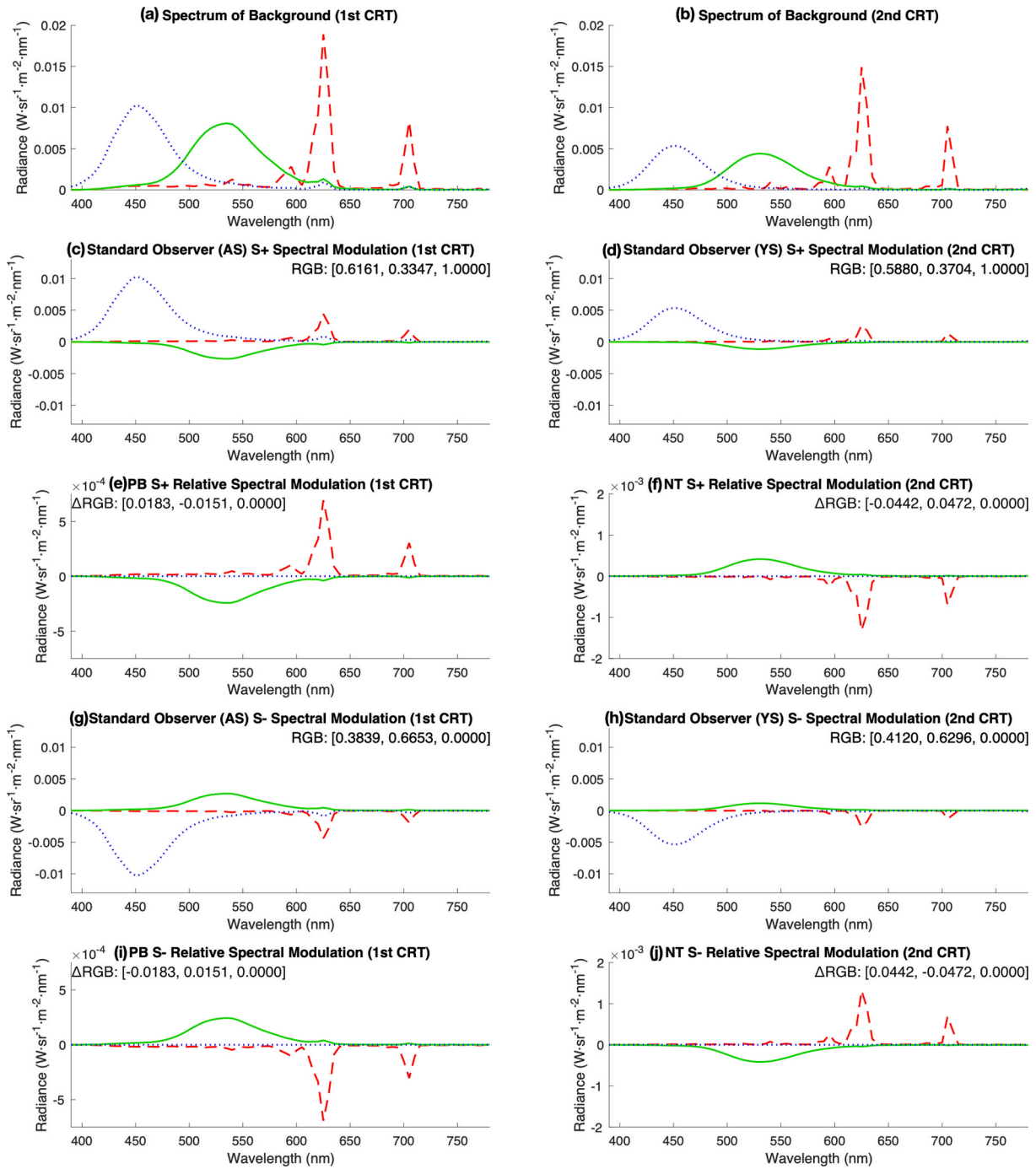


Fig. A2. CRT radiance spectra and modulations of it. Note the different vertical axis scales across panels. The left column plots are from the first monitor used in the experiment, and the right column plots are from the second one. (a-b) The mid-gray backgrounds ($[R, G, B] = [0.5, 0.5, 0.5]$) on both monitors). (c-d) The modulations of the RGB channels required to produce S+ (at maximum contrast) relative to mid-gray background for Stockman-Sharp observers (AS, YS). This RGB triplet represents the modulations of the 3 channels, with $[0.5, 0.5, 0.5]$ representing no modulation, normalized to a unit cube (so that at least one modulation is 0 or 1). (e-f) For non-Stockman-Sharpe observers PB and NT, the RGB triplet *change* relative to the RGB used for Stockman-Sharp observers for S+ at maximum contrast (e.g., for PB the red channel modulation was $0.6161 + 0.0183$). (g-h) The corresponding S- condition for standard observers. (i-j) The corresponding S- condition for non-standard observers.

Appendix B. Constant noise model

MLDS results

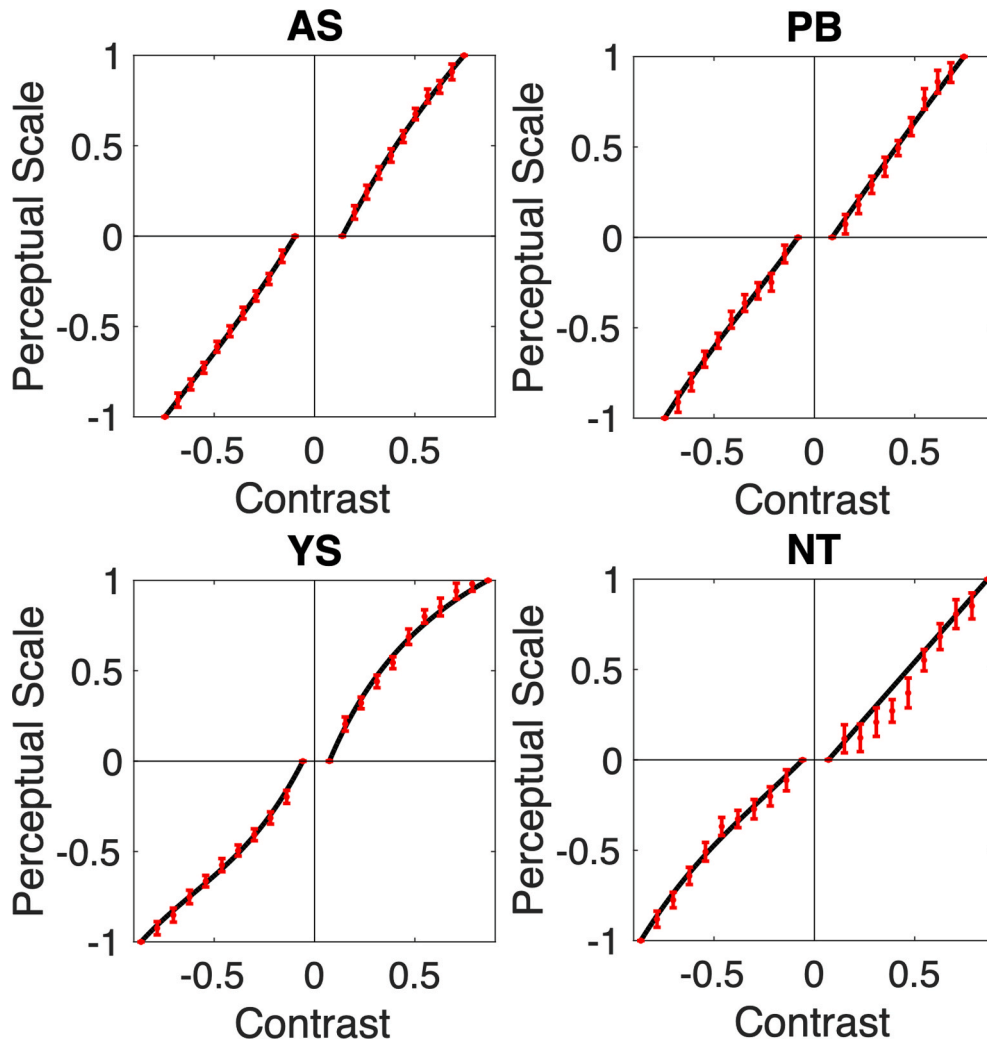


Fig. B1. Constant noise MLDS for S cone contrast fitted results from four participants. See in the main text for explanation.

Fig. B1 shows the results from the MLDS experiment. The original MLDS model (Maloney & Yang, 2003) was applied to the same dataset as in the Results section to generate estimates of perceptual scale values and the corresponding (constant) standard deviation of the internal noise. The fitted perceptual scale values are almost identical to the variable noise model results shown in Fig. 2.

Discrimination results

The results of the discrimination experiment are shown in Fig. B2 as red data points; they are the same as in Fig. 3. In each observer's panel, the S+ pedestal results are plotted on the right side, and the S- pedestal results are plotted on the left side.

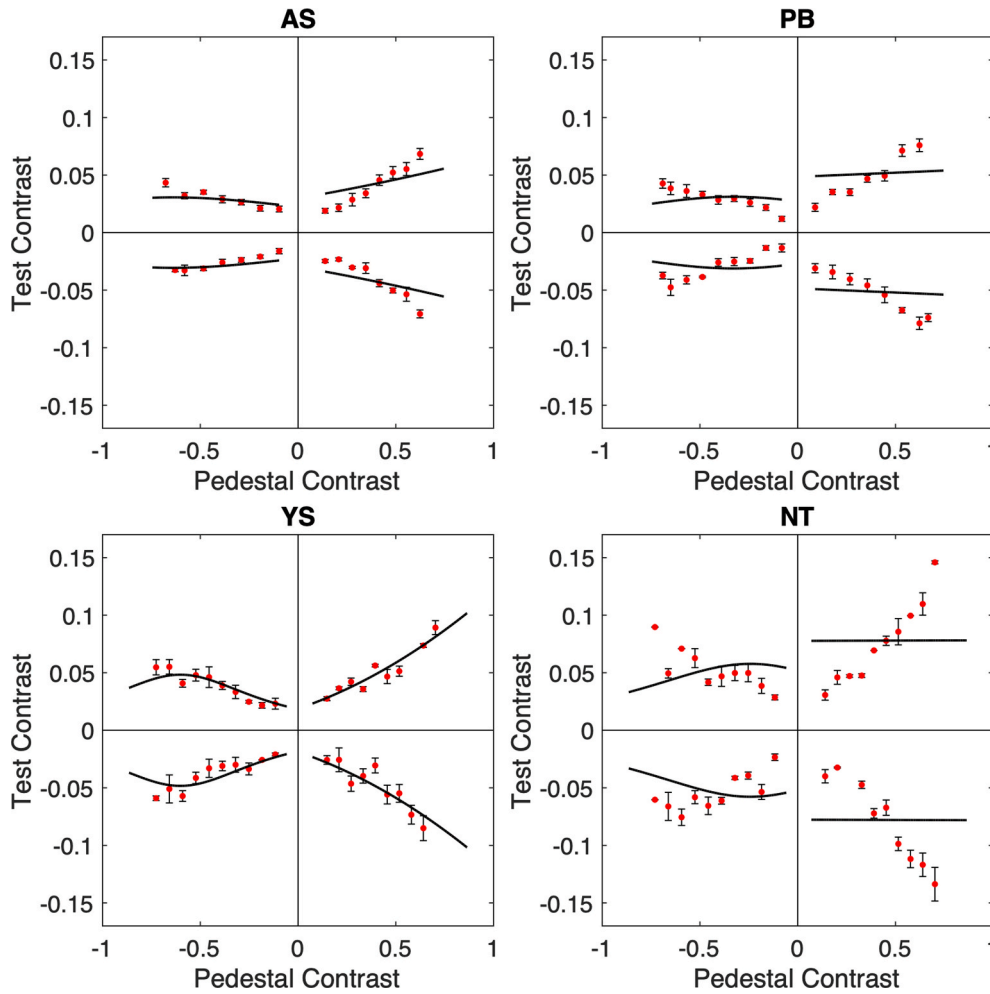


Fig. B2. S cone pedestal discrimination results with the constant-noise model prediction, in the same format as in the main text. The black curves are prediction model fit results, using the constant-noise MLDS model.

Applying previous prediction model to discrimination results

The constant noise prediction model shown here in [Appendix B](#) is the same as in previous work (Shi & Eskew, 2024). The model used constant noise perceptual scale curves to predict pedestal discrimination thresholds. Equation [B\(1\)](#) summarizes this model, where C_t represents discrimination threshold contrast; $\sigma_{S_{\pm}}$ represents the constant internal noise estimated by the MLDS model (the constancy of the noise is the only difference from Eq. [\(1\)](#) in the main text); $\frac{d}{dc}P(C_{ped})$ represents the slope of the perceptual scale curve at pedestal contrast C_{ped} ; The only free parameter to be fit to the thresholds is $k_{S_{\pm}}$.

$$C_t = k_{S_{\pm}} \times \sigma_{S_{\pm}} \times \frac{1}{\frac{d}{dc}P(C_{ped})} \tag{B1}$$

The black curves in [Fig. B2](#) show the predictions based on applying this model directly to the constant-noise perceptual scales shown in [Fig. B1](#). Except for the S+ data of observer YS, none of the prediction curves fit the discrimination results well. The fit is especially bad for observers PB and NT, whose perceptual scales were nearly linear, so the prediction curves are almost horizontal lines (see [Section 4.1 and 4.4](#) in the main text). This linearity also leads to the goodness of fit being near zero. The fitted parameters are summarized in [Table B1](#). [Table B2](#) presents the goodness of fit of these prediction curves (R^2 , RMSE). Note that PB and NT's S- R^2 values are negative, showing that the conventional calculation of R^2 cannot be interpreted as the proportion of variance explained by this nonlinear model. The negative R^2 values indicate that the model fit is worse than using the data's mean (a horizontal line) as the predicted thresholds. Unlike in the case of achromatic increments and decrements (Shi & Eskew, 2024), the model based upon constant noise fails to relate S cone MLDS and discrimination.

Table B1
Parameters of constant noise MLDS model.

		AS	PB	YS	NT
S+	σ_{s_+}	0.075	0.116	0.074	0.171
	m_{s_+}	2.170	13.908	0.724	326.704
	k_{s_+}	0.955	0.676	0.833	0.575
S-	σ_{s_-}	0.067	0.111	0.073	0.104
	n_{1,s_-}	0.430	0.651	1.397	0.665
	n_{2,s_-}	-0.826	-0.642	-2.524	-0.484
	n_{3,s_-}	1.963	1.631	2.449	1.155
	n_{4,s_-}	-0.183	-0.129	-0.134	-0.066
	k_{s_-}	0.658	0.397	0.613	0.575

Table B2
Measures of goodness of fit to constant noise model.

Condition/Observer	AS	PB	YS	NT
S+, R^2	0.55	0.14	0.85	0.005
S+, RMSE	0.011	0.017	0.008	0.034
S-, R^2	0.48	-0.18	0.72	-0.71
S-, RMSE	0.005	0.011	0.007	0.021

Appendix C. Achromatic data reanalysis with variable noise

In this appendix, the achromatic MLDS and pedestal discrimination data from Shi and Eskew (2024) were re-analyzed using the variable noise MLDS and prediction model proposed in the current paper. Figs. C1 and C2 serve the same purpose as Figs. 2 and 3, or Figs. B1 and B2, showing the MLDS model and prediction model analysis results. Tables C1 and C2 serve the same purpose as Tables 1 and 2, or Tables B1 and B2, showing the parameters fit of the models, and the goodness of fit.

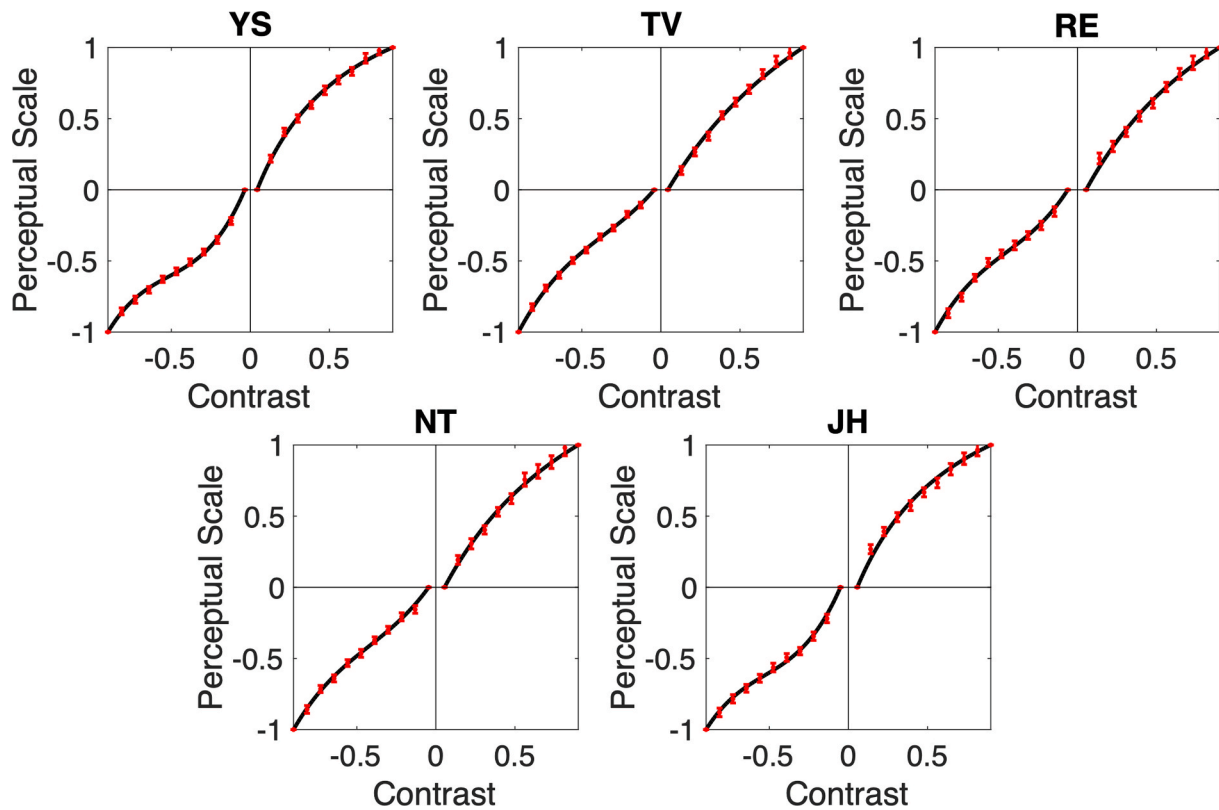


Fig. C1. Variable noise MLDS model results using the achromatic judgments from Shi and Eskew (2024).

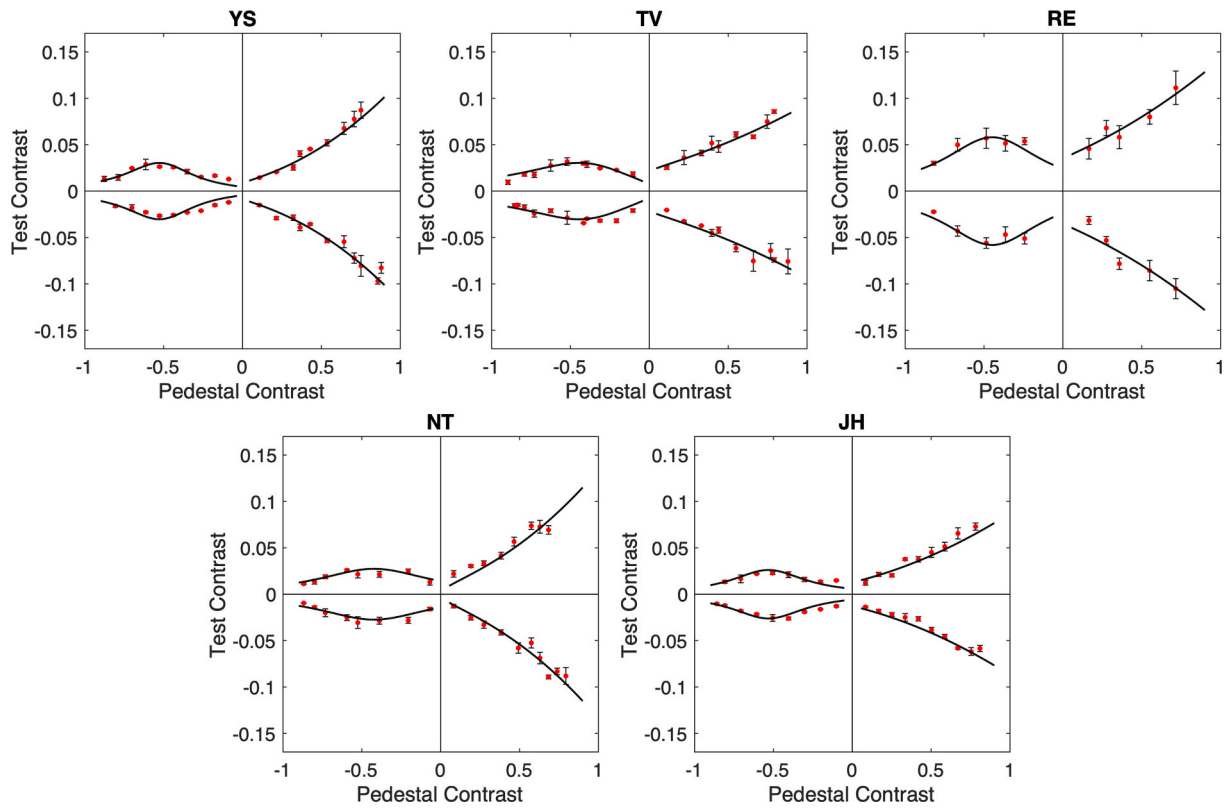


Fig. C2. Variable noise prediction model results applied to the achromatic discrimination thresholds from Shi and Eskew (2024).

Although the model *allows* the noise to be variable in this version, the slopes of the noise function (parameter a_{\pm} in Eq. (1)) for most observers and conditions (both polarities for JH, RE, A- for YS and NT) are 0 or are very close to it, which indicates that in these conditions, the noise is nearly constant (and is given by b_{\pm} in Eq. (1)). This corresponds to the previous analysis in Shi and Eskew (2024), in which the constant noise model predicts discrimination well.

Another thing worth noting is that the perceptual scales produced by MLDS with the potentially-variable noise (Eq. (1)) are identical to the original perceptual scales that assumed constant noise (Shi & Eskew 2024, Eq. (3)). This is consistent with Kingdom’s (2016) finding that MLDS is ‘internal-noise-free’, but it is also the case that the noise obtained when fitting Eq. (1) to our difference judgments was nearly constant, and so this model is effectively the same as the constant noise model used in Shi and Eskew (2024).

Table C1

Parameters of variable noise model on achromatic data from Shi and Eskew (2024).

		YS	TV	RE	NT	JH
A+	a_{A+}	0.026	0.022	0.009	0.109	0
	b_{A+}	0.028	0.041	0.068	0	0.064
	m_{A+}	0.614	1.437	1.169	1.096	0.676
	k_{A+}	0.935	1.006	1.141	0.741	0.630
A-	a_{A-}	0.020	0.042	0	0	0
	b_{A-}	0.030	0.011	0.059	0.049	0.056
	$n_{1,A-}$	2.880	1.412	1.979	1.532	2.721
	$n_{2,A-}$	-4.471	-1.523	-2.656	-1.945	-4.340
	$n_{3,A-}$	2.909	1.401	2.025	1.703	2.967
	$n_{4,A-}$	-0.097	-0.056	-0.114	-0.074	-0.139
	k_{A-}	0.405	0.690	0.830	0.494	0.308

Table C2

Measures of goodness of fit of variable noise model on achromatic data from Shi and Eskew (2024).

Condition/Observer	YS	TV	RE	NT	JH
A+, R^2	0.95	0.90	0.88	0.91	0.92
A+, RMSE	0.006	0.006	0.008	0.007	0.005
A-, R^2	0.47	0.64	0.74	0.74	0.55
A-, RMSE	0.004	0.004	0.006	0.003	0.003

Data availability

Data will be made available on request.

References

- Aguilar, G., Wichmann, F. A., & Maertens, M. (2017). Comparing sensitivity estimates from MLDS and forced-choice methods in a slant-from-texture experiment. *Journal of Vision*, 17(1), 37. <https://doi.org/10.1167/17.1.37>
- Aguilar, M., & Stiles, W. S. (1954). Saturation of the Rod Mechanism of the Retina at High Levels of Stimulation. *Optica Acta: International Journal of Optics*, 1(1), 59–65. <https://doi.org/10.1080/713818657>
- Ala-Laurila, P., Greschner, M., Chichilnisky, E. J., & Rieke, F. (2011). Cone photoreceptor contributions to noise and correlations in the retinal output. *Nature Neuroscience*, 14(10), 1309–1316. <https://doi.org/10.1038/nn.2927>
- Angueyra, J. M., & Rieke, F. (2013). Origin and effect of phototransduction noise in primate cone photoreceptors. *Nature Neuroscience*, 16(11), 1692–1700. <https://doi.org/10.1038/nn.3534>
- Baudin, J., Angueyra, J. M., Sinha, R., & Rieke, F. (2019). S-cone photoreceptors in the primate retina are functionally distinct from L and M cones. *eLife*, 8, Article e39166. <https://doi.org/10.7554/eLife.39166>
- Calkins, D. J. (2001). Seeing with S cones. *Progress in Retinal and Eye Research*, 20(3), 255–287. [https://doi.org/10.1016/S1350-9462\(00\)00026-4](https://doi.org/10.1016/S1350-9462(00)00026-4)
- Chatterjee, S., & Callaway, E. M. (2002). S Cone Contributions to the Magnocellular Visual Pathway in Macaque Monkey. *Neuron*, 35(6), 1135–1146. [https://doi.org/10.1016/S0896-6273\(02\)00874-7](https://doi.org/10.1016/S0896-6273(02)00874-7)
- Dacey, D. M., Crook, J. D., & Packer, O. S. (2014). Distinct synaptic mechanisms create parallel S-ON and S-OFF cone opponent pathways in the primate retina. *Visual Neuroscience*, 31(2), 139–151. <https://doi.org/10.1017/S0952523813000230>
- Devinck, F., & Knoblauch, K. (2012). A common signal detection model accounts for both perception and discrimination of the watercolor effect. *Journal of Vision*, 12(3), 19. <https://doi.org/10.1167/12.3.19>
- Eiber, C. D., Pietersen, A. N. J., Zeater, N., Solomon, S. G., & Martin, P. R. (2018). Chromatic summation and receptive field properties of blue-on and blue-off cells in marmoset lateral geniculate nucleus. *Vision Research*, 151, 41–52. <https://doi.org/10.1016/j.visres.2017.09.002>
- Estévez, O., & Spekreijse, H. (1982). The “silent substitution” method in visual research. *Vision Research*, 22(6), 681–691. [https://doi.org/10.1016/0042-6989\(82\)90104-3](https://doi.org/10.1016/0042-6989(82)90104-3)
- Farnsworth, D. (1943). The Farnsworth-Munsell 100-Hue and Dichotomous Tests for Color Vision*. *Journal of the Optical Society of America*, 33(10), 568. <https://doi.org/10.1364/JOSA.33.000568>
- Gabree, S. H., Shepard, T. G., & Eskew, R. T., Jr. (2018). Asymmetric high-contrast masking in S cone increment and decrement pathways. *Vision Research*, 151, 61–68. <https://doi.org/10.1016/j.visres.2017.06.017>
- García-Pérez, M., & Alcalá-Quintana, R. (2007). The transducer model for contrast detection and discrimination: Formal relations, implications, and an empirical test. *Spatial Vision*, 20(1–2), 5–43. <https://doi.org/10.1163/156856807779369724>
- García-Pérez, M., & Alcalá-Quintana, R. (2009). Fixed vs. variable noise in 2AFC contrast discrimination: Lessons from psychometric functions. *Spatial Vision*, 22(4), 273–300. <https://doi.org/10.1163/156856809788746309>
- Georgeson, M. A., & Meese, T. S. (2006). Fixed or variable noise in contrast discrimination? The jury’s still out.... *Vision Research*, 46(25), 4294–4303. <https://doi.org/10.1016/j.visres.2005.08.024>
- Hartline, H. K. (1938). The Response of Single Optic Nerve Fibers of the Vertebrate Eye to Illumination of the Retina. *American Journal of Physiology-Legacy Content*, 121(2), 400–415. <https://doi.org/10.1152/ajplegacy.1938.121.2.400>
- He, J., Taveras-Cruz, Y., & Eskew, R. T., Jr. (2021). Modeling individual variations in equiluminance settings. *Journal of Vision*, 21(7), 15. <https://doi.org/10.1167/jov.21.7.15>
- Ijekah, R., Vanston, J. E., & Crognale, M. A. (2019). Mechanisms contributing to increment threshold and decrement threshold spectral sensitivities. *Vision Research*, 158, 157–163. <https://doi.org/10.1016/j.visres.2019.03.004>
- Kim, Y. J., Packer, O., & Dacey, D. M. (2024). A circuit motif for color in the human foveal retina. *Proceedings of the National Academy of Sciences*, 121(36), Article e2405138121. <https://doi.org/10.1073/pnas.2405138121>
- Kingdom, F. A. A. (2016). Fixed versus variable internal noise in contrast transduction: The significance of Whittle’s data. *Vision Research*, 128, 1–5. <https://doi.org/10.1016/j.visres.2016.09.004>
- Klug, K., Herr, S., Ngo, I. T., Sterling, P., & Schein, S. (2003). Macaque Retina Contains an S-Cone OFF Midget Pathway. *The Journal of Neuroscience*, 23(30), 9881–9887. <https://doi.org/10.1523/JNEUROSCI.23-30-09881.2003>
- Knoblauch, K., & Maloney, L. T. (2008). MLDS: Maximum Likelihood Difference Scaling in R. *Journal of Statistical Software*, 25(2). <https://doi.org/10.18637/jss.v025.i02>
- Kontsevich, L. L., Chen, C.-C., & Tyler, C. W. (2002). Separating the effects of response nonlinearity and internal noise psychophysically. *Vision Research*, 42(14), 1771–1784. [https://doi.org/10.1016/S0042-6989\(02\)00091-3](https://doi.org/10.1016/S0042-6989(02)00091-3)
- Maloney, L. T., & Yang, J. N. (2003). Maximum likelihood difference scaling. *Journal of Vision*, 3(8), 5. <https://doi.org/10.1167/3.8.5>
- McLellan, J. S., & Eskew, R. T., Jr. (2000). ON and OFF S-cone pathways have different long-wave cone inputs. *Vision Research*, 40(18), 2449–2465. [https://doi.org/10.1016/S0042-6989\(00\)0107-3](https://doi.org/10.1016/S0042-6989(00)0107-3)
- Packer, O. S., Verweij, J., Li, P. H., Schnapf, J. L., & Dacey, D. M. (2010). Blue-Yellow Opponency in Primate S Cone Photoreceptors. *The Journal of Neuroscience*, 30(2), 568–572. <https://doi.org/10.1523/JNEUROSCI.4738-09.2010>
- Patel, A. S., & Jones, R. W. (1968). Increment and Decrement Visual Thresholds. *Journal of the Optical Society of America*, 58(5), 696. <https://doi.org/10.1364/JOSA.58.000696>
- Patterson, S. S., Kuchenbecker, J. A., Anderson, J. R., Bordt, A. S., Marshak, D. W., Neitz, M., & Neitz, J. (2019). An S-cone circuit for edge detection in the primate retina. *Scientific Reports*, 9(1), 11913. <https://doi.org/10.1038/s41598-019-48042-2>
- Schiller, P. H. (1992). The ON and OFF channels of the visual system. *Trends in Neurosciences*, 15(3), 86–92. [https://doi.org/10.1016/0166-2236\(92\)90017-3](https://doi.org/10.1016/0166-2236(92)90017-3)
- Schiller, P. H. (2010). Parallel information processing channels created in the retina. *Proceedings of the National Academy of Sciences*, 107(40), 17087–17094. <https://doi.org/10.1073/pnas.1011782107>
- Shi, Y., & Eskew, R. T., Jr. (2024). Asymmetries between achromatic increments and decrements: Perceptual scales and discrimination thresholds. *Journal of Vision*, 24(4), 10. <https://doi.org/10.1167/jov.24.4.10>
- Shoener, C., & Mullen, K. T. (2022). Linking perceived to physical contrast: Comparing results from discrimination and difference-scaling experiments. *Journal of Vision*, 22(1), 13. <https://doi.org/10.1167/jov.22.1.13>
- Smithson, H. E. (2014). S-cone psychophysics. *Visual Neuroscience*, 31(2), 211–225. <https://doi.org/10.1017/S0952523814000030>
- Stockman, A., & Sharpe, L. T. (2000). The spectral sensitivities of the middle- and long-wavelength-sensitive cones derived from measurements in observers of known genotype. *Vision Research*, 40(13), 1711–1737. [https://doi.org/10.1016/S0042-6989\(00\)00021-3](https://doi.org/10.1016/S0042-6989(00)00021-3)
- Sun, H., Smithson, H. E., Zaidi, Q., & Lee, B. B. (2006). Specificity of Cone Inputs to Macaque Retinal Ganglion Cells. *Journal of Neurophysiology*, 95(2), 837–849. <https://doi.org/10.1152/jn.00714.2005>
- Szmajda, B. A., Buzás, P., FitzGibbon, T., & Martin, P. R. (2006). Geniculocortical relay of blue-off signals in the primate visual system. *Proceedings of the National Academy of Sciences*, 103(51), 19512–19517. <https://doi.org/10.1073/pnas.0606970103>
- Tailby, C., Solomon, S. G., & Lennie, P. (2008). Functional Asymmetries in Visual Pathways Carrying S-Cone Signals in Macaque. *The Journal of Neuroscience*, 28(15), 4078–4087. <https://doi.org/10.1523/JNEUROSCI.5338-07.2008>
- Takasaki, H. (1966). Lightness Change of Grays Induced by Change in Reflectance of Gray Background. *Journal of the Optical Society of America*, 56(4), 504. <https://doi.org/10.1364/JOSA.56.000504>
- Wang, Q., Richters, D. P., & Eskew, R. T. (2014). Noise masking of S-cone increments and decrements. *Journal of Vision*, 14(13), 8. <https://doi.org/10.1167/14.13.8>
- Weber, A. I., Shea-Brown, E., & Rieke, F. (2021). Identification of Multiple Noise Sources Improves Estimation of Neural Responses across Stimulus Conditions. *ENEURO*, 8(4), Article ENEURO.0191-21.2021. <https://doi.org/10.1523/ENEURO.0191-21.2021>
- Webster, M. A., & Mollon, J. D. (1994). The influence of contrast adaptation on color appearance. *Vision Research*, 34(15), 1993–2020. [https://doi.org/10.1016/0042-6989\(94\)90028-0](https://doi.org/10.1016/0042-6989(94)90028-0)
- Wetherill, G., & Levitt, H. (1965). Sequential estimation of points on a psychometric function. *British Journal of Mathematical and Statistical Psychology*, 18(1), 1–10. <https://doi.org/10.1111/j.2044-8317.1965.tb00689.x>
- Whittle, P. (1992). Brightness, discriminability and the “Crispening Effect.”. *Vision Research*, 32(8), 1493–1507. [https://doi.org/10.1016/0042-6989\(92\)90205-W](https://doi.org/10.1016/0042-6989(92)90205-W)
- Wickens, T. D. (2002). *Elementary signal detection theory*. Oxford: Oxford Univ. Press. <https://doi.org/10.1093/acprof:oso/9780195092509.001.0001>
- Wool, L. E., Packer, O. S., Zaidi, Q., & Dacey, D. M. (2019). Connectomic Identification and Three-Dimensional Color Tuning of S-OFF Midget Ganglion Cells in the Primate Retina. *The Journal of Neuroscience*, 39(40), 7893–7909. <https://doi.org/10.1523/JNEUROSCI.0778-19.2019>